LOCALIZATION FOR A CAR-LIKE MOBILE ROBOT USING NONLINEAR DYNAMIC MODEL

Niramon Ruangpayoongsak, Hubert Roth and Robert Mayr
Institute of Automatic Control Engineering, University of Siegen, Hoelderinstr. 3, D-57068 Siegen, Germany

Keywords: Localization, Mobile robotics, Kalman filter, Dynamic model.

Abstract: The problem of localization is well known in mobile robotics. A solution is to use a model-based technique such as a kalman filter with multi sensor data fusion. For a car-like mobile robot, the nonlinear dynamic model is suitable for robot movement representation. This work presents the discrete extended kalman filter including a nonlinear dynamic model for the mobile robot localization. As inputs for the kalman filtering, gyroscope and compass sensors provide the relative and absolute yaw angles. The experiments are performed on several path types and the averages of the final position errors and the final heading errors are proposed.

1 INTRODUCTION

The localization problem is a well known important problem in mobile robotics. No matter how the environment is or how the functionalities of the robot are, whether the robot navigates autonomously or semi-autonomously, it is useful to know where the robot is. The mobile robot localization can be classified into two main categories that are relative (local) localization and absolute (global) localization as described in (Goel et.al., 1999).

For large scale outdoor environment, the positioning resolution is effective to have absolute localization regarding disturbances resulting from a missing smoothness of the ground surface. The absolute positioning sensors such as global positioning system (GPS), differential GPS, beacon system, natural landmarks are exploited with the relative positioning sensors e.g. gyroscope to obtain accurate robot position. On the other hand, in indoor environment with a smooth and flat surface, the disturbance is small. However, the satellite signals in buildings with many walls often fail regarding to weakness and blindness. Therefore, a good performance of at least relative localization is necessary.

Sensors used for relative positioning are e.g. odometer, compass and gyroscope. These sensors have different strength and weakness (Nehmzow, 2003). Odometer is a common device used to provide travelled distances. The relative position provided by odometers has sometimes an accumulated error from wheel slippage. The gyroscope and compass sensors provide the yaw angle. The gyroscope measures angular velocity. The integration of this signal provides the relative yaw angle. The gyroscope has a drift in measurement. The compass sensor provides the ready-to-use absolute yaw angle.

The robot's nonlinear dynamic model realization and the robot localization using discrete extended kalman filter is proposed. The comparison of the real robot position and heading errors by using odometer, gyroscope, and compass sensor are presented.
This paper is organized as follows: Section 2 explains the robot modelling, section 3 describes the extended kalman filter, section 4 shows the calculation of robot estimated positions and headings, section 5 presents the experimental results while section 6 contains the conclusion.

2 ROBOT MODELLING

The first step in model based localization is to develop a suitable mathematical model for the robot. When considering the structure of the mobile robot, it is a four wheel vehicle with the driving principle of a car, steering the front wheels and propelling the rear wheels. The nonlinear dynamic model

Ruangpayoongsak N., Roth H. and Mayr R. (2005).
LOCALIZATION FOR A CAR-LIKE MOBILE ROBOT USING NONLINEAR DYNAMIC MODEL.
In *Proceedings of the Second International Conference on Informatics in Control, Automation and Robotics - Robotics and Automation*, pages 367-372
DOI: 10.5220/0001176803670372
Copyright © SciTePress

represents the dynamic movement of the robot with the nonlinear characteristics of the side force at the wheels. This property has majority effect when the car moves along curvature path. In the following, the nonlinear dynamic model is introduced and subsequently the application on the mobile robot is described.

2.1 Nonlinear dynamic model

The nonlinear dynamic mathematical model for a four wheel vehicle was determined as a single track model describing transverse and longitudinal dynamics, neglecting roll and pitch angles and comprising front and rear wheels to one fictitious wheel (Riekert and Schunck, 1940, Mayr, 1991).

Fig. 1 shows the dynamic variables of a vehicle as follows:

- the yaw angle ψ, vehicle orientation,
- the yaw velocity ψ', the first derivative of the yaw angle,
- the longitudinal velocity v,
- the sideslip angle β,
- the actual position X and Y of the center of gravity in Cartesian coordinates,
- the front side force S_v and the rear side force S_h,
- the rear longitudinal forces H resulting from the driving motor,
- the steering angle δ_v.

In addition, there are the following constants: Vehicle mass m, moment of inertia θ and the distances l_v (l_h) between the front (rear) wheels and the longitudinal axes of the car.

Based on the balance of the forces acting on the vehicle in the longitudinal and lateral directions, the torques and the kinematic conditions, the nonlinear dynamic vehicle model is presented as follows:

$$\dot{\beta} = \dot{\psi} - \frac{1}{mv}\{(H-T)\sin\beta + S_h\cos\beta\} - \frac{1}{mv}\{S_v\cos(\beta+\delta)\} \quad (1)$$

$$\dot{\psi} = \psi' \quad (2)$$

$$\ddot{\psi} = \frac{1}{\theta}(S_v l_v\cos\delta - S_h l_h) \quad (3)$$

$$\dot{v} = \frac{1}{m}\{(H-T)\cos\beta - S_h\sin\beta\} - \frac{1}{m}\{S_v\sin(\beta+\delta)\} \quad (4)$$

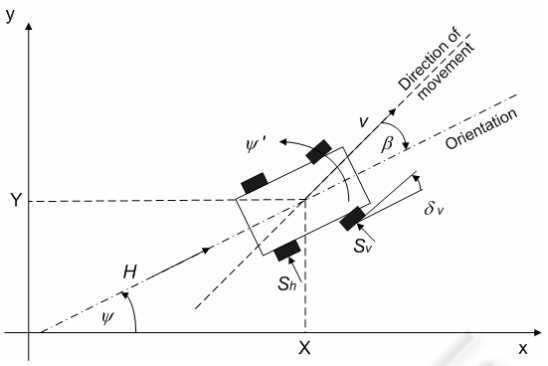

Figure 1: Dynamical variables of the vehicle

The front and rear side forces S_v and S_h of the vehicle depend on the slip angles α_v and α_h, while α_v depends itself also on the steering angle δ_v. The nonlinear functions Γ_v and Γ_h determine the dynamics in the tires as follows:

$$S_v = \Gamma_v(\alpha_v) \quad (5)$$

$$S_h = \Gamma_h(\alpha_h) \quad (6)$$

By these functions representing a characteristic line, the behavior of the wheels and the tires is taken into consideration. This characteristic line includes limitations and descending behavior for high values in the argument. As shown in Fig. 2, here the functions are approximated by three straight lines describing the dependence of side force values S on their argument α. For low arguments, a nearly proportional ascend of the side force can be recognized, while beyond the value α_{max} the side force is descending. At α_{max} the value for the corresponding side force reaches its maximum. The area below α_{max} is called the ascending part, while the area, where the side force descends is called the descending part of the characteristic line. As a

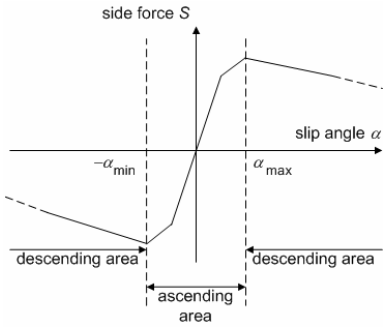

Figure 2: Characteristic line Γ of the wheels and tyres

consequence of the gradual inverse dynamics, the car would begin to skid when driving in the descending part. During a normal maneuver without skidding, every wheel of the vehicle is working in the ascending area of the characteristic line. This nonlinear characteristic coming from automotive technology is also applicable to a car-like mobile robot in indoor environment over dry and flat floor.

As here, high absolute values for α_v and α_h will never come up, the functions Γ_v and Γ_h can be simplified to the amplification factors c_v and c_h. Then, (5) and (6) result in

$$S_v = c_v \alpha_v = c_v \left(\beta - \frac{l_v}{v} \dot{\psi} + \delta \right) \tag{7}$$

$$S_h = c_h \alpha_h = c_h \left(\beta + \frac{l_h}{v} \dot{\psi} \right) \tag{8}$$

2.2 Model realization

The mobile experimental robot for locomotion and intelligent navigation (MERLIN) has been designed and developed for both, indoor and outdoor environments. The sensors onboard are odometer, gyroscope, 3D compass, ultrasonic sensor, infrared sensor, and bumper as shown in Fig. 3. The semi-autonomous tele-control using joystick and path commands are available via internet (Kuhle et. al., 2004).

The moment of inertia from calculation is equal to 0.169167 kg·m^2. The side force constants c_v and c_h are from experiments. By keeping a constant steering angle δ_v and a constant driving motor force H, the robot drives on a circular path with a constant speed and the robots position is externally recorded by a V-scope™ positioning sensor. The data are exploited with the model equations to obtain the side force constant. The results are c_v = 168450 and c_h = 152290. The length from the center of gravity to the front wheels is l_v = 0.15 meter and to the rear wheels l_h = 0.15 meter. The mass of the robot is m = 7 kg including the batteries. Due to the surface of the robot is small and as the robot drives with low speed, the air resistance is neglected.

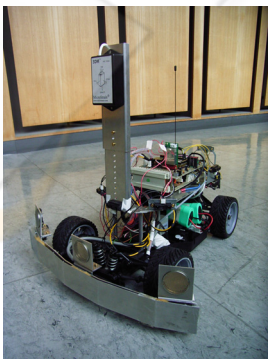

Figure 3: MERLIN

3 EXTENDED KALMAN FILTER (EKF)

The kalman filter is a model-based sensor fusion technique. Two main processes are time update and measurement update. For a nonlinear dynamic system, the discrete extended kalman filter is applied (Brown, 1983, Welch and Bishop, 2002). Assume that a nonlinear process has a state vector $x \in \Re^n$ and is governed by the non-linear stochastic differential equation with a measurement $z \in \Re^m$ that is

$$x_k = f(x_{k-1}, u_{k-1}, w_{k-1}), \tag{9}$$

$$z_k = h(x_k, v_k), \tag{10}$$

where w_k and v_k represent the process and measurement noise. After linearization, the linearized state transition matrix is represented without noises. The Jacobian matrix of the partial derivatives of f with respect to x is

$$A_{[i,j]} = \frac{\partial f_{[i]}}{\partial x_{[j]}} (\hat{x}_{k-1}, u_k, 0), \tag{11}$$

where the state vector x is

$$x = [\beta \quad \psi \quad \psi' \quad v]^T, \tag{12}$$

and the Jacobian matrix of partial derivatives of h with respect to x is

$$H_{[i,j]} = \frac{\partial h_{[i]}}{\partial x_{[j]}} (\tilde{x}_k, 0), \tag{13}$$

where h is

$$h = [x_1 \quad x_2 \quad x_3 \quad x_4]^T. \tag{14}$$

The kalman filtering process starts from initialization of all state variables and matrices. Assume that the process and measurement noises are Gaussian with zero mean and are constant throughout the process. The priori estimate state variable $\hat{x}_k^-$ and the priori estimate error covariance P_k^- at time step k are

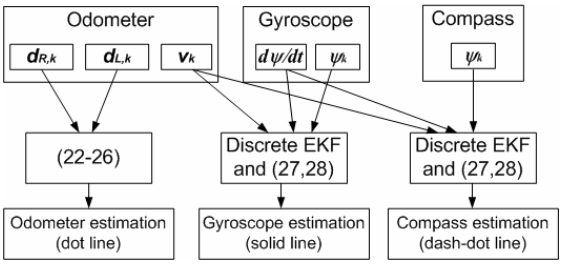

Figure 4: Architecture of the robot localization system

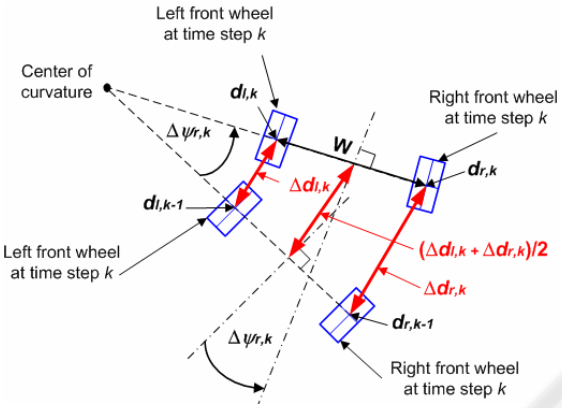

Figure 5: Variables based on odometer (cont.)

$$\hat{x}_k^- = f(\hat{x}_{k-1}, u_k, 0), \quad (15)$$

$$P_k^- = A_k P_{k-1} A_k^T + Q, \quad (16)$$

where Q is the process noise constant matrix. After that the kalman gain K_k, the posteriori estimate state variable $\hat{x}_k$, and the posteriori estimate error covariance P_k are calculated as follows:

$$K_k = P_k^- H_k^T (H_k P_k^- H_k^T + R)^{-1}, \quad (17)$$

$$\hat{x}_k = \hat{x}_k^- + K_k (z_k - h(\hat{x}_k^-, 0)), \quad (18)$$

$$P_k = (I - K_k H_k) P_k^-, \quad (19)$$

where R is the measurement noise covariance.

The inputs of the robot model are the steering angle δ and the driving motor force H. Let the input vector at time step k be

$$u_k = [\delta_k \quad H_k]^T, \quad (20)$$

and let the measurement vector be

$$z_k = [z_{\beta,k} \quad z_{\psi,k} \quad z_{\psi',k} \quad z_{v,k}]^T, \quad (21)$$

where $z_{\beta,k}$, $z_{\psi,k}$, $z_{\psi',k}$, and $z_{v,k}$ are the measured values of the state variables at time step k. As the robot drives very slow and, thus, the sideslip angle, which is difficult to sense, is of minor importance, the measurement value of the sideslip is set to zero for all time steps k. Regarding the system model in (1–4), the discrete system is first obtained using Euler's method (Franklin, 1998). The process and measurement noise covariance matrices Q and R are tuned off-line in the simulation for appropriate value and kept constant during the iterative process. The selected values are $1x10^{-6}$ for all diagonal matrix elements.

4 POSITION AND HEADING CALCULATIONS

As shown in Fig. 4, three different estimated paths are from using measurement of odometer, gyroscope, and compass estimation. The odometer estimated position and heading is the non-model based whereas the other two estimations are based on kalman filter and the nonlinear dynamic model.

4.1 Odometer position and heading estimation

The position $x_{odo,k}$, $y_{odo,k}$ and heading $\psi_{odo,k}$ at step k are calculated from

$$x_{odo,k} = x_{odo,k-1} + \left(\frac{\Delta d_{R,k} + \Delta d_{L,k}}{2}\right)\cos\psi_{odo,k}, \quad (22)$$

$$y_{odo,k} = y_{odo,k-1} + \left(\frac{\Delta d_{R,k} + \Delta d_{L,k}}{2}\right)\sin\psi_{odo,k}, \quad (23)$$

$$\psi_{odo,k} = \psi_{odo,k-1} + \tan^{-1}\left(\frac{\Delta d_{R,k} - \Delta d_{L,k}}{W}\right), \quad (24)$$

$$\Delta d_{R,k} = d_{R,k} - d_{R,k-1}, \quad (25)$$

$$\Delta d_{L,k} = d_{L,k} - d_{L,k-1} \quad (26)$$

where $\Delta d_{R,k}$ is the difference of driven distances of the right wheel between the time steps k and k-1 as shown in Fig. 5. Note that similar calculation is applied to the difference of distances left $\Delta d_{L,k}$. Here, $d_{L,k}$ represents the already driven distance of the left wheel at time step k, while $d_{R,k}$ is the driven distance of the right wheel. These driven distances since the beginning of the ride can be computed from the amount of pulses from the odometer on each wheel. The wheel base W is the distance between the center

of the left wheel to the center of the right wheel and is equal to 23.5 cm.

4.2 Position and heading estimation using gyroscope and compass

The estimated positions of the relative yaw angle of the gyroscope and absolute yaw angle of the compass are calculated by using

$$x_k = st \cdot v_k \cos(\psi_k - \beta_k) + x_{k-1}, \quad (27)$$

$$y_k = st \cdot v_k \sin(\psi_k - \beta_k) + y_{k-1}, \quad (28)$$

where v_k, ψ_k, and β_k are posterior estimated state variables as in (18). The estimated robot heading is ψ_k. st is the time step. Here also the kalman filtering is applied.

5 EXPERIMENTAL RESULTS

The experiments were performed in indoor and the sensor data were collected for off-line plots using MATLAB. All graphs scale has unit in meter and the data sampling rate is 0.2 sec. The test is designed for testing the performance of localization when the robot moves straight on, in a curve path, and the combination of both.

5.1 Test results

As already mentioned, in order to improve the quality of the measurement signals, the data coming from the gyroscope as well as the data from the compass was subsequently processed by the kalman filter using the measured velocity signal from the odometer.

Odometer: Please note that for comparison, the data coming from the odometer itself (dot line) is plotted directly using (22-26) and, thus, not updated by the kalman filter. Due to (24), (25) and (26), relevant odometer data is not only the average of the wheel movements but also the difference of the movements of the left and right wheel in order to get information about the change of orientation of the robot.

Gyroscope: The measured yaw angle by gyroscope are applied as inputs to kalman filter measurement updates and the positions are obtained from (27) and (28) shown as solid line. Please note, that here the odometer only provides the measurement value for the velocity.

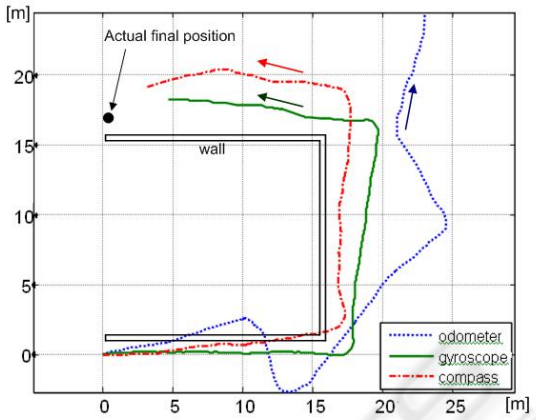

Figure 6: Wall-path estimated positions

Compass: Similarly, by using the compass yaw angle with kalman filter, the position estimation from (27) and (28) are represented by dash-dot line. Please note, that here also the odometer only provides the measurement value for the velocity.

The wall-path is shown in Fig. 6. At the wall corners, the robot turns with minimum radius curve. The estimated final position using odometer has sometimes large error as shown in the figure. The gyroscope has drift in some trials whereas the compass result is quite static for all trials with error of deviation in measurement as in line path.

For every path type, several driving tests were performed. Regarding each driving test, the real final position determined was compared to the position value measured by the on-board sensors and the resulting errors were calculated. Subsequently, the

Table 1: Average position errors (e_{pos})

	Odometer (meters)	Compass (meters)	Gyroscope (meters)
Rectangular	0.71	0.33	**0.17**
U	0.88	0.38	**0.12**
Arcs	**0.26**	0.32	0.29
Line1	0.53	**0.27**	1.02
Line2	**0.19**	0.78	0.27
Wall	15.09	**3.35**	5.44

Table 2: Average heading errors ($e_{heading}$)

	Odometer (degrees)	Compass (degrees)	Gyroscope (degrees)
Rectangular	-23	14	**-1**
U	7	12	**2**
Arcs	6	110	**1**
Line1	**5**	61	6
Line2	5	-91	**0**
Wall	-58	-52	**-10**

average error values result from the averages of the respective errors of all similar driving tests.

The average errors in position and heading are summarized in Tables 1 and 2, respectively. The position error e_{pos} is the error between the actual final position and the estimated final position. Based on the actual and estimated values for the yaw angle, the heading error $e_{heading}$ is the error of robot heading at the final position. These errors are calculated by

$$e_{pos} = \sqrt{\bar{e}_x^{\,2} + \bar{e}_y^{\,2}}, \tag{29}$$

$$e_{heading} = \frac{\sum_{i=1}^{n} \left(\psi_{estimate,i} - \psi_{actual,i} \right)}{n}, \tag{30}$$

Where $\bar{e}_x$ and $\bar{e}_y$ are the mean of error in x and y direction from several driving tests. $\psi_{estimate,i}$ and $\psi_{actual,i}$ are the estimated and actual final heading of test number i, respectively.

In Table 1, the average of final position errors of gyroscope are not the largest in all trajectories. Due to the localization based on model, the position errors of compass and gyro are not much different. The gyro and compass with discrete EKF outperforms the odometer positioning for wall path. As in Table 2, the average of final heading errors of the well calibrated gyroscope present the excellent performance over compass and odometer.

5.2 Discussions

For the line1 path, both average position and heading errors of gyroscope are larger than those of odometer and compass. This presents the minority performance of the gyroscope over the odometer in line1 path by the mechanical structure of the robot.

For the trajectories containing arcs path that are rectangular, U, and arcs path, the yaw angle measurement dominates in the position estimation process. The well calibrated gyroscope presents good performance without drift. Nevertheless, for the large scale scenario as for wall path, the gyroscope provides good estimation, because here the drift is not relevant.

The compass yaw angle deviation occurs in all trajectories. This error shows up in most of all the driving tests. The average errors of final heading for all trajectories in Table 2 are in most cases larger. However, there are some cases that the deviation doesn't exist as shown in Fig. 6.

For the odometer estimated position, the large error is presented in the wall path. This error is caused by the slippage in the wheels and does not always occur in all driving tests. However, the final position and heading errors are larger than those of the gyroscope, except in line1 and line2 trajectories regarding to the previous discussion of the error in the estimation using gyroscope.

6 CONCLUSIONS

The discrete extended kalman filter is applied to a car-like mobile robot for improvement of localization using the nonlinear dynamic model. The experiments are performed on six path types and the final position error and final heading error using odometer, gyroscope, and compass data are compared. The well calibrated gyroscope provides minority performance in robot final position for line1 path. For the other five path types, the gyroscope position errors are smaller than those of odometer and the in performance in final heading of the gyroscope dominates the compass and odometer for all trajectories.

REFERENCES

Brown, R.G., 1983. *Introduction to random signal analysis and kalman filtering*, John Wiley & Sons, USA, p. 300.

Franklin, G. F., Powell, J. D., and Workman, M., 1998. *Digital Control of Dynamic Systems*, 3rd edition, Addison Wesley Longman, p. 59.

Goel, P. and Roumeliotis, S. I. and Sukhatme, G. S., 1999. Robot Localization Using Relative and Absolute Position Estimates *In Proc. 1999 IEEE/RSJ International Conference on Intelligent Robots and Systems*, Kyongju, Korea, Oct. 17-21, pp. 1134-1140.

Kuhle, J., Roth, H., Ruangpayoongsak, N., 2004. MOBILE ROBOTS and airships in a multi-robot team. *The 1st IFAC Symposium on Telematics Applications in Automation and Robotics*, Helsinki University of Technology, Finland, pp. 67-72.

Mayr, R., 1991. *Verfahren zur Bahnfolgeregelung für ein automatisch geführtes Fahrzeug*, Dissertation, University of Dortmund, Dortmund, Germany.

Nehmzow, U., 2003. *Mobile Robotics: A Practical Introduction*, 2nd Edition, Springer-Verlag, London.

Riekert, P. and Schunck, T.E., 1940. Zur Fahrmechanik des gummibereiften Kraftfahrzeugs. *Ing. Arch.*, Vol. XI, pp. 210-224.

TWelch, G., and Bishop, G., 2002. *An Introduction to the Kalman Filter*, UNC-Chapel Hill, USA, TR 95-041.T